

# Numerical study of three-dimensional wind flow over grain storage bunkers

Wei He<sup>1</sup>, Liang Cheng<sup>1</sup>, Ming Zhao<sup>1</sup>, James Darby<sup>2</sup> and Greg Hopkins<sup>3</sup>

<sup>1</sup>School of Civil and Resource Engineering,  
The University of Western Australia, 35 Stirling Highway, Crawley, WA 6009, Australia

<sup>2</sup>CSIRO Entomology,  
GPO Box 1700, Canberra, ACT 2601, Australia

<sup>3</sup>ABB Grain,  
GPO Box 1169, Adelaide, SA 5001, Australia

## Abstract

In Australia, grain storage bunkers fitted with covering tarpaulins are widely used. Tarpaulin billowing takes place when it is windy. It is well known that billowing has negative impacts on the life span of a tarpaulin, but also has positive effects on phosphine transport throughout the grain stack during fumigation. It is suspected that preventing billowing during fumigation would retard phosphine distribution to such an extent that contemporary phosphine dispensing protocols risk failure. Mathematically, a moving boundary condition that could represent wind induced tarpaulin billowing presents a challenging technical problem and has not been published.

In this study, three-dimensional wind flow around a grain storage bunker is investigated by finite element method (FEM) based computational fluid dynamics (CFD) modelling, as the first step towards quantifying tarpaulin billowing. The Petrov-Galerkin finite element method (PG-FEM) is used to solve the three-dimensional Reynolds-Averaged Navier-Stokes (RANS) equations with a  $k-\omega$  turbulent closure. This study is focused on the wind induced pressure distribution and fluctuation on bunker surface at a relatively low Reynolds number of 2,000. The simplification of flow from three-dimensional to two-dimensional at the mid span of the bunker was discussed with cross flow wind direction.

## Introduction

Tarpaulin covered bunkers are commonly adopted in Australia as a cost-effective method to store grains in an open yard. It is estimated that over 50% of grains are stored by this means accordingly. Generally, insect infestation of grain in bunkers is controlled by phosphine fumigation. The effectiveness of bunker fumigation is largely determined by the wind induced environment around bunkers and the associated pressure differentials across the bunker boundaries. Phosphine is dispensed at several positions along the walls of a bunker, via aluminium phosphide tablets or direct injection of phosphine gas in gas cylinders. The dispensing points are limited to reduce intervention with the weather proof finish of the tarpaulin to wall joints, while maximising operator safety and convenience. Distribution of phosphine gas throughout the grain in the bunker occurs due to passive processes, such as wind infiltration, convection and molecular diffusion. For adequate insect control, phosphine concentrations need to be maintained at adequate levels for over 14 days throughout the bunker. However, in certain areas concentrations are not achieved or maintained due to wind effects primarily, especially far away from phosphine dispensing source. Nevertheless, it is recognised that the wind induced tarpaulin billowing is a key mechanism for the transport of phosphine gas throughout the bunker.

In order to understand the interaction between turbulent wind flow and tarpaulin billowing, the grain storage bunker is simplified as a surface-mounted bluff body with rigid boundaries. Pressure distribution and fluctuation are simulated under certain wind conditions. In this study, the numerical method is introduced as the first step to quantitatively measure the wind flow patterns and characteristics around bunkers. Flow around surface-mounted obstacles with different shapes was intensively studied during the past two decades in experiments [2, 3] and numerical modelling, especially in the case of flow around a surface-mounted cube, due to its simple geometry but complex flow structures. The flow has been employed as a benchmarking case to validate numerical turbulent modelling. Among these numerical studies, methods like RANS with different turbulent models [4, 5], Large Eddy Simulations (LES) [1, 5, 6] and Direct Numerical Simulation (DNS) [9] were validated against the experiment data.

In the current work, the numerical model was firstly validated against experimental data of flow over the surface-mounted cube. Then, the validated model was applied to simulate flow over a bunker.

## Governing equations and numerical method

Figure 1 shows the sketch of wind past a grain bunker in non-dimensional coordinate systems. The wind direction is perpendicular to the long axis of the bunker. The non-dimensional parameters are defined as

$$(x, y, z)_i = (x', y', z')_i / W \quad (1)$$

$$(u, v, w) = (u', v', w') / U \quad (2)$$

$$t = Ut' / W \quad (3)$$

$$Re = UW / \nu \quad (4)$$

where  $W$  is the width of the bunker,  $U$  is the wind speed at the top level of the bunker walls ( $z=H$ ),  $\nu$  is the kinetic viscosity of fluid,  $x$ ,  $y$  and  $z$  are Cartesian coordinates,  $u$ ,  $v$  and  $w$  are fluid velocity components in  $x$ ,  $y$  and  $z$  direction respectively,  $p$  is the pressure,  $t$  is the time.

The governing equations that consist of three-dimensional incompressible RANS equations, the continuity equation and the  $k-\omega$  equations [8], are solved by using Petrov-Galerkin finite element method developed by [10, 11].

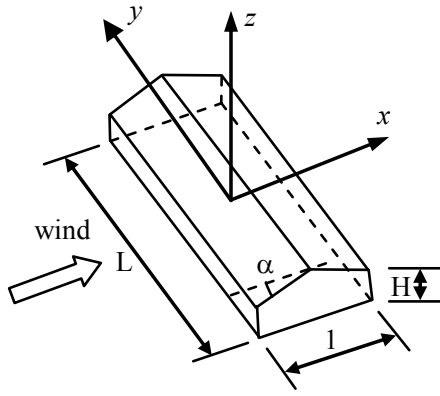


Figure 1. Sketch of wind flow past a grain bunker in non-dimensional size

### Numerical model validation

The numerical model was validated against the experimental results of flow around a surface-mounted cube that independent experimental data are well documented. Figure 2 shows the computational domain. The length scale is non-dimensionalized by the boundary length of the cube  $H$ . Flow parameters are same as those used in the experiment in [2]. The Reynolds number based on the inflow velocity  $U$  and cubic boundary length is  $Re=40,000$ , and the domain height is  $2H$ . The size of the computational domain is  $7H$  in cross flow direction and  $10H$  in flow direction. The centre of the cube is located  $3H$  downstream from the inlet boundary. The fully developed turbulent flow condition was applied at the inlet boundary. The structured mesh has 900,000 nodes. Symmetric boundary condition is prescribed at two lateral boundaries, and the non-slip boundary condition for floor and ceiling boundaries and cube surfaces. On the symmetric boundary, the velocity component perpendicular to the boundary is zero and the velocity component tangential to the boundary is calculated according to the momentum equation.

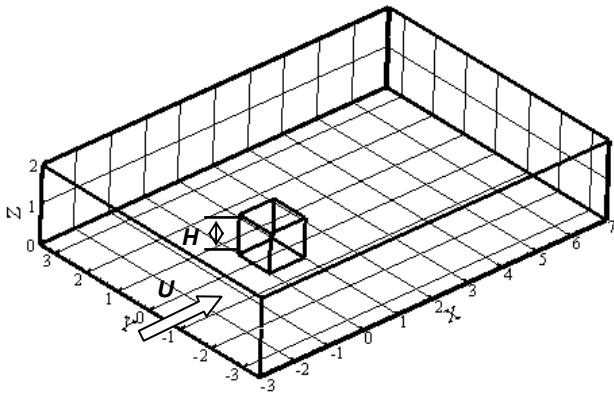


Figure 2. Non-dimensional computational domain for flow past a cube

Vortex shedding is observed in the numerical results and the Strouhal number is assessed to be 0.152, which is close to the experimental results of 0.145 [2]. Figure 3 shows the streamlines based on the phase-averaged horizontal velocity at the level of  $z=0.01$ . The simulated flow structure is quite similar to what was observed in the test. Figure 4 shows the distribution of streamwise phase-averaged velocity at two vertical lines in  $xz$ -plane. The velocity at the line of  $x=1$  is smaller than the test data below  $z=1.5$ . Further refining mesh did not improve the result. Future work still needs to be done to improve the accuracy of the model.

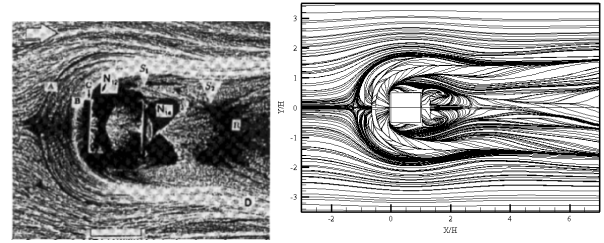


Figure 3. Streamlines on the floor (Experimental data on left hand side from [2])

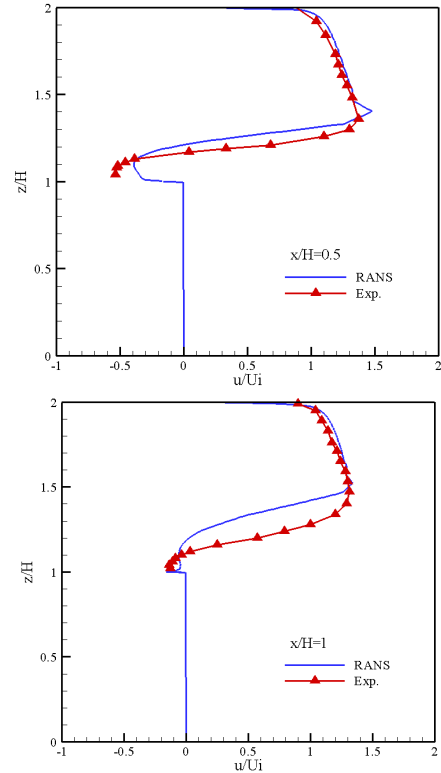


Figure 4. Velocity component in streamwise direction at  $y=0$  in comparison with experimental data

### Flow over bunkers

It is expected that the fluctuation of the pressure on top of the tarpaulin leads to the tarpaulin billowing. The Reynolds number is set to be 2,000 when wind flow over a grain bunker is studied. This low Reynolds number is used based on the consideration that the accuracy of the results can be guaranteed at affordable mesh density. The bunkers' length to width ratio ( $L$ ) is set at 3 and 20 respectively in the simulation. The level of the ridge of the bunker is  $z=0.5$ , the height of front and rear wall is  $H=0.3$ . The roof slope is  $\tan\alpha=0.4$ . Figure 5 shows the finite element mesh around the bunker for  $L=3$ . In the simulation a fully developed boundary layer flow are given at the inlet boundary. At the two lateral boundaries and the top boundary, the symmetric boundary condition is applied. Mesh dependence study was carried out and it is found that further refining the mesh makes negligible difference on the results.

This study is focused on the pressure distribution around the bunker surface. The pressure coefficient  $C_p$ , is defined as

$$C_p = (p - p_0) / (\rho U^2 / 2) \quad (5)$$

where  $p_0$  is the pressure at the inlet boundary. Figure 6 shows the time series of the pressure at a number of locations at the section of  $y=0$  of the bunker for  $L=3$ . Figure 6 (a) defines the locations of

the pressure monitoring points. As shown in Figure 6, the pressure on bunker surface is fluctuating with time and its mean value varies along the bunker surface. Figure 7 and 8 show the pressure coefficient distribution along the bunker surface. It can be seen that both the mean value and the root-mean-square (r.m.s.) value of the pressure have large gradients near the two ends. The largest root mean square (r.m.s.) of  $C_p$  occurred on the rear wall.

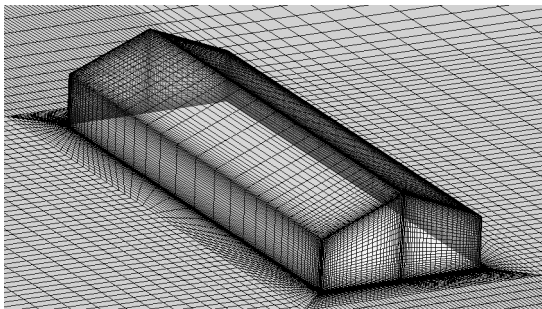


Figure 5. Finite element mesh on bunker surface

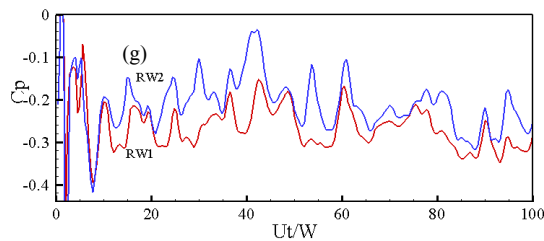
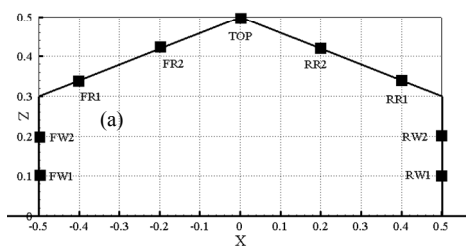


Figure 6. Time histories of the pressure coefficients on symmetry plane (a) locations of monitoring points at the section of  $y=0$ ; (b) – (g) pressure time series

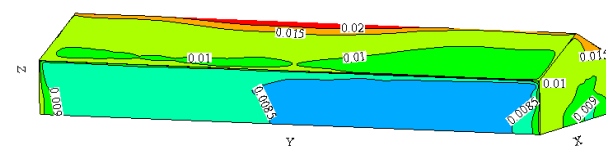
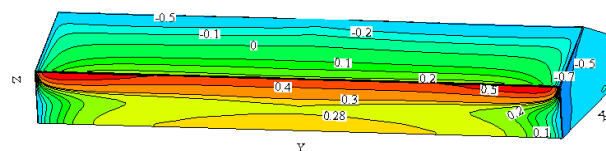


Figure 7. Time-averaged (top figure) and r.m.s. of  $C_p$  (bottom figure) on windward bunker surface for  $L=3$  (upstream side)

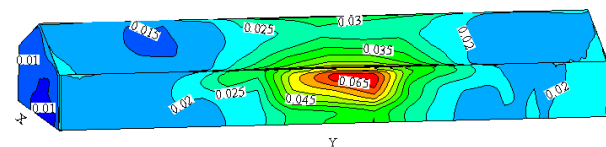
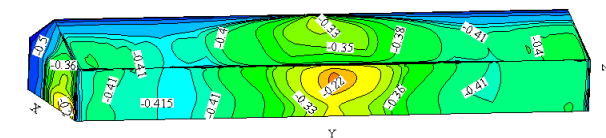
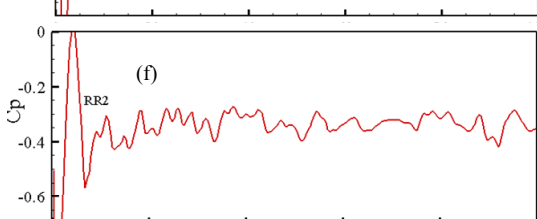
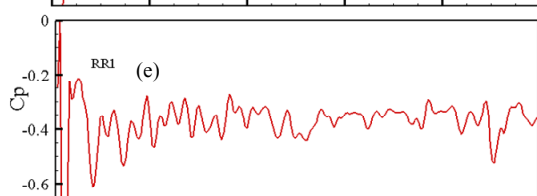
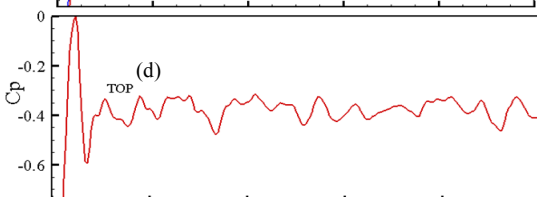
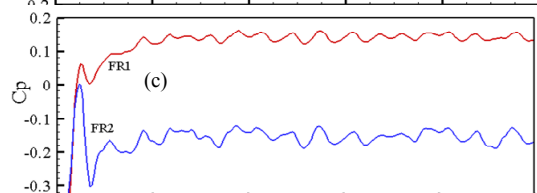
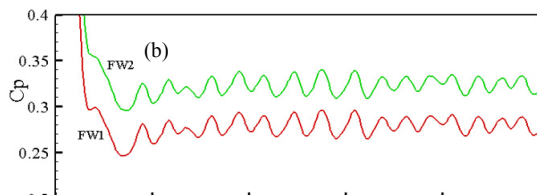


Figure 8. Time-averaged (top figure) and r.m.s.  $C_p$  (bottom figure) on leeward bunker surface for  $L=3$  (lee side)

When flow past a bunker with large length to width aspect ratio of  $L=20$ , only half of the physical domain bunker is chosen as the computational domain as shown in Figure 9. The symmetric boundary condition is specified in  $y = 0$  plane.

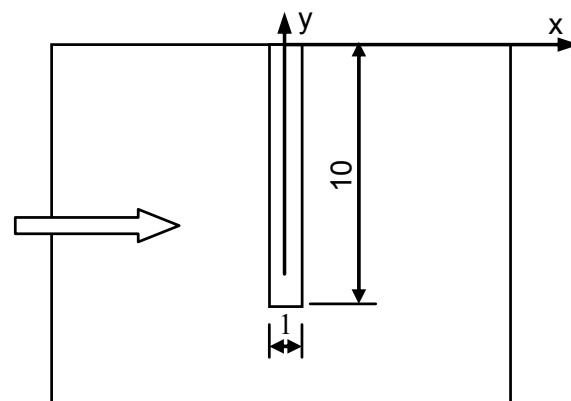


Figure 9. Bunker with symmetric boundary at  $y=0$

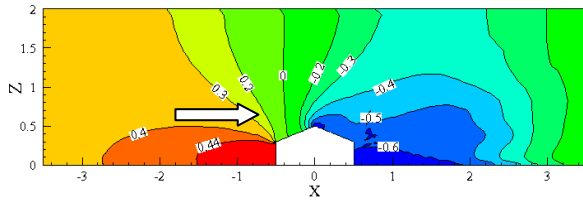


Figure 10. The time-averaged  $C_p$  of wind flow on the symmetric plane of  $y=0$

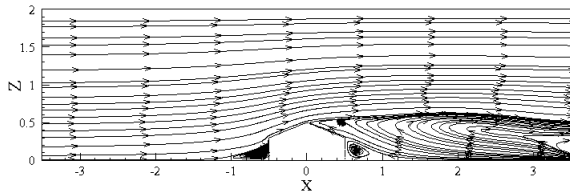


Figure 11. The streamlines on the symmetric plane of  $y=0$

On the symmetry plane, the pressure distribution and flow streamline around the bunker are plotted in Figure 10 and Figure 11. The time-averaged  $C_p$  in the front wall of the bunker appears to be larger than that when  $L=3$ .

Figure 12 shows the pressure distribution along three lateral lines (in  $y$ -direction). The locations of FW1, FR1 and RR1 defined in Figure 6 (a) are typical. The pressure coefficients have large gradient close to the end ( $y= -10$ ) of bunker. The pressure coefficients do not vary along the cross-stream direction in the middle part of the bunker ( $-6 < y < 0$ ). It indicates that the ends of the bunker only affect the flow in the zone of  $-10 < y < -6$ .

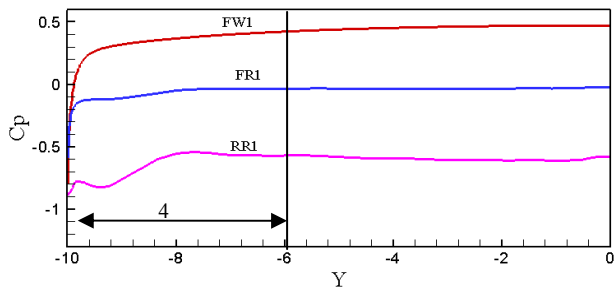


Figure 12. Time-averaged  $C_p$  in lateral direction

## Conclusions

In the present study, three-dimensional wind flow past a bunker is investigated numerically. The numerical model was firstly validated against experimental data of flow around a surface-mounted cube and numerical solutions are compared quantitatively well with experimental data. In order to ensure the accurate results at affordable computational time, simulations are carried out at relatively low Reynolds number. Results are summarised as below:

1. Wind induced pressure on bunker surface fluctuates with time, as indicated in the r.m.s contour. Both mean value of pressure and r.m.s value of pressure vary very much close to the two ends.
2. The Reynolds-averaged pressure on the windward surface is mainly determined by bunker's geometric form. However, on the leeward surface, it is also influenced by the near wake vortex, especially approaching to the two ends of the bunker in lateral directions.

3. Three-dimensionality of the mean pressure and r.m.s pressure are limited to two-ends of bunkers in the lateral direction. The wind flow within the mid span 4 times of bunker width away from each end is of two-dimensional characteristics.
4. The tarpaulin billowing phenomenon is mostly affected by the pressure fluctuation on the roof of the bunker. It is estimated that the frequency and amplitude of fluctuations are largely related to bunkers' orientation, geometric configuration, and the turbulent intensity in the atmospheric boundary layer. Further studies will be carried out to quantify those factors.
5. This study is carried out at a low Reynolds number. The applicability of the results to the high Reynolds number case needs to be verified further.

## Acknowledgement

The author would like to acknowledge the support from the Co-operative Research Centre for National Plant Biosecurity (Australia), project number 50091.

## References

- [1]. Krajnovic, S. & Davidson, L., Large-Eddy Simulation of the Flow around a Bluff Body. *Aiaa J*, **40**, 2002, 927-936.
- [2]. Martinuzzi, R. & Tropea, C., The Flow around Surface-Mounted, Prismatic Obstacles Placed in a Fully-Developed Channel Flow. *J Fluid Eng-T Asme*, **115**, 1993, 85-92.
- [3]. Hussein, H.J. & Martinuzzi, R.J., Energy Balance for Turbulent Flow around a Surface Mounted Cube Placed in a Channel. *Phys Fluids*, **8**, 1996, 764-780.
- [4]. Iaccarino, G., Ooi, A., Durbin, P.A. & Behnia, M., Reynolds Averaged Simulation of Unsteady Separated Flow. *Int J Heat Fluid Fl*, **24**, 2003, 147-156.
- [5]. Rodi, W., Comparison of Les and Rans Calculations of the Flow around Bluff Bodies. *J Wind Eng Ind Aerod*, **71**, 1997, 55-75.
- [6]. Shah, K.B. & Ferziger, J.H., A Fluid Mechanicians View of Wind Engineering: Large Eddy Simulation of Flow Past a Cubic Obstacle. *J Wind Eng Ind Aerod*, **67-8**, 1997, 211-224.
- [7]. Wilcox, D.C., Reassessment of the Scale-Determining Equation for Advanced Turbulence Models. *Aiaa J*, **26**, 1988, 1299-1310.
- [8]. Wilcox, D.C., Simulation of Transition with a 2-Equation Turbulence Model. *Aiaa J*, **32**, 1994, 247-255.
- [9]. Yakhot, A., Anor, T., Liu, H.P. & Nikitin, N., Direct Numerical Simulation of Turbulent Flow around a Wall-Mounted Cube: Spatio-Temporal Evolution of Large-Scale Vortices. *J Fluid Mech*, **566**, 2006, 1-9.
- [10]. Zhao, M., Cheng, L., Teng, B. & Dong, G., Hydrodynamic Forces on Dual Cylinders of Different Diameters in Steady Currents. *J Fluid Struct*, **23**, 2007, 59-83.
- [11]. Zhao, M., Cheng, L. & Zhou, T.M., Direct Numerical Simulation of Three-Dimensional Flow Past a Yawed Circular Cylinder of Infinite Length. *J Fluid Struct*, **25**, 2009, 831-847.